Feasibility study of an active infrared scanning system for thermal detection of buried antipersonnel landmines. Part II: performance analysis in realistic situations.

MARCO BALSI[a], MASSIMO CORCIONE[b,*] and PIERPAOLO DELL'OMO[b]
[a] Dipartimento di Ingegneria Elettronica
[b] Dipartimento di Fisica Tecnica
University of Rome "La Sapienza", via Eudossiana 18
00184 Rome, Italy
*corresponding author e-mail address: massimo.corcione@uniroma1.it

Abstract: The detection performance of the new method for thermal sensing of buried anti-personnel landmines discussed in part I of the paper was evaluated under simplified hypotheses, as the effects of neither the soil non-homogeneity, nor the climate, were taken into account. Indeed, real soils are non-homogeneous, which can affect the response of the ground to thermal stimulation, and also both solar irradiation and air temperature changes may introduce non-negligible noise in the temperature distribution of the soil surface. The performance of the method proposed is then evaluated with reference to more realistic environmental situations through a specifically developed time-implicit computer-code. The main result obtained is that, once the double information carried out by the evolution along the scanning line of both the temperature and its time-derivative is analysed, the system proposed proves to be able to ensure good detection capabilities also in noisy background. Constructional aspects of the device, and possible extension of the basic architecture, are also proposed and discussed.

Keywords: AP landmines; Thermal detection; Numerical study; Non-homogeneous soil; Climatic changes.

1 Introduction

Infrared thermal detection is one of the most promising technologies for buried mine location, in terms of both efficiency and availability of equipment. The basic principle underlying mine thermal detection is the difference in thermal conduction properties of explosives with respect to the soil, which may give rise to anomalies in the temperature distribution of the ground surface above the buried mine when the soil is heated, either naturally by solar irradiation, or artificially. Main drawbacks of existing thermal detection methods are the long investigation-times required, as well as the relatively low contrasts of surface temperature, which make difficult to ensure safe location of all buried mines.

A new method for thermal detection of buried anti-personnel landmine, based on the use of a focused radiant heat source and a contactless thermometer mounted on a suspended carriage scanning the ground surface, has been introduced and studied numerically in part I of the paper, in which encouraging results were obtained under simplified hypotheses. In fact, the effects of neither the soil non-homogeneity, nor the climatic diurnal cycles, were taken into account.

Indeed, non-homogeneity of real soils may produce non-negligible noise in the surface temperature data, known as background clutter, thus making the real field scenario more complex than that reproduced in the first-approach study performed in part I of the paper. In addition, also the solar irradiation and air temperature changes occurring during the de-mining operations, may have non-negligible effects on the detection capability of thermal systems. As far as traditional thermal methods for buried mine detection are concerned, recent studies on the effects due to the background clutter [1–4] and on the effects of the climatic diurnal cycles [5–9] are readily available in the open literature.

In this framework, aim of the present part II of the paper is to carry out a numerical analysis of the detection performance of the active-scanning device proposed, when working in environmental situations more realistic than those assumed in part I, i. e., by taking into due account both soil non-uniformity and climate effects. Main constructional aspects of the device are also discussed, and possible extensions of the basic architecture are proposed.

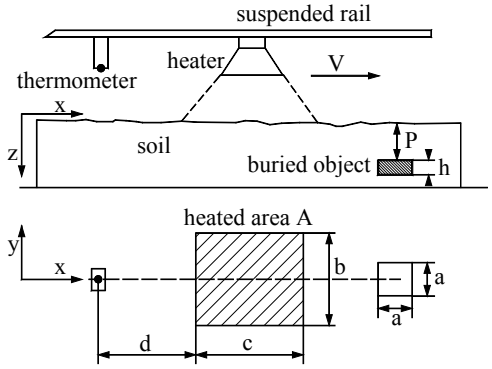

Fig. 1. Sketch of the thermal detector and target geometry

2 Mathematical formulation and solution method

The same 5cm x 5cm x 2cm anti-personnel landmine considered in part I of the paper, supposed being made of a homogeneous material with k_m = 0.4W/mK, and $(\rho c)_m$ = 1.53x10 ^{6}J/m^{3}K, is buried at a depth P in a dry, non-homogeneous soil. The non-uniformity of the soil properties is simulated by assuming that, in each discretization volume of the whole integration domain, both the thermal conductivity k_s and the volumetric heat capacity $(\rho c)_s$ of the soil vary linearly at random around the uniform values used in part I of the paper, i.e., 0.75 W/mK, and 1.53x10^6 J/m^{3}K, respectively, within a percent range of ±30%, with no correlation to the values pertaining to the adjacent control volumes. The ±30% range of variability is considered large enough to give an adequate first-approch representation of soils with a considerable degree of non-homogeneity. In addition, real climatic conditions are assumed, which means that the effects of both solar irradiation and air temperature changes during the investigation-time are accounted for. In particular, reference is e. g. made to summer typical Mediterranean climates, assuming that the peak of the incoming solar radiation per unit area above the horizontal plane is 750W/m^2, which occurs at noon, and that the air temperature has a daily oscillation of 10°C around a mean value of 30°C.

The detection performance of the system proposed, which moves at constant velocity V and delivers infrared heating power to the ground surface upon an area A = b × c, as sketched in Fig. 1, is again evaluated through the study of the time-evolution of the temperature field, which is described by the energy flow equation:

$$k\nabla^2 T = c\rho\frac{\partial T}{\partial \tau} \tag{1}$$

Equation (1) is solved through the same control volume formulation of the finite difference method described in full details in part I, across the same integration domain, and making use of the same discretization grid.

The study is subdivided into two consecutive steps:

1) a first-step analysis, in which only the effects of the soil non-homogeneity are evaluated, so as to determine in what measure the detection system is able to distinguish between a buried landmine and a more or less abrupt change in the soil composition, i. e., between mines and non-mines signatures;

2) a second-step analysis, in which the effects of climate are successively added, so as to obtain a description more adherent to real situations; in this case, the effects produced by the use of a multi-thermometer scanning device on the reliability of the results obtained are also evaluated.

The following boundary conditions are used:

a) energy balance at any i-th discretization element of the ground surface, which takes into account the solar energy absorbed, the infrared radiant energy absorbed and emitted, the energy exchanged with air by convective heat transfer, and the energy conducted to the soil:

$$a_{s-sun}\delta_{s-sun}W_{sun} + a_{s-IR}\delta_{s-IR}W = \\ = \sigma\varepsilon(T^4 - T_{mr}^4) + h_c(T - T_a) - k\frac{\partial T}{\partial z} \tag{2}$$

b) heat flux continuity at any interface between the i-th and the j-th adjacent control volumes:

$$-k_i\left.\frac{\partial T}{\partial n}\right|_i = -k_j\left.\frac{\partial T}{\partial n}\right|_j \tag{3}$$

c) zero temperature gradient, i.e., zero heat transfer rate, at the four side-surfaces of the 3D Cartesian integration domain, which are chosen at sufficiently large distance from the landmine:

$$\frac{\partial T}{\partial n} = 0 \tag{4}$$

d) zero temperature gradient, i.e., zero heat transfer rate, at a depth H =1m at which the thermal effects of both the artificial soil heating and the solar irradiation can be neglected, as shown by a series of preliminary test specifically performed:

$$\left.\frac{\partial T}{\partial z}\right|_{z=H} = 0 \tag{5}$$

where W_{sun} is the incoming solar power per unit area; W is the infrared power delivered to the

ground surface per unit area; ε is the emissivity of the ground surface in the long-wave IR, which is reasonably assumed equal to 0.9; $a_{s\text{-}sun}$ is the ground surface coefficient of absorption of the solar radiation, which is assumed equal to 0.4; $a_{s\text{-}IR}$ is the ground surface coefficients of absorption of the long-wave IR radiation, which is assumed equal to ε, i.e., 0.9, under the assumption that in the long-wave IR the soil behaves like a grey-body; $\delta_{s\text{-}sum}$ is a Boolean factor equal to unity or zero, according as the effects of solar radiation are accounted for or not; $\delta_{s\text{-}IR}$ is a Boolean factor equal to unity or zero, according as the ground surface element being considered is irradiated or not by the heater; σ is the Stefan-Boltzmann constant, equal to 5.67×10^{-8} W/(m^{2}K^4); T_a is the air temperature, which may be assumed either equal to 20°C along the entire investigation-time, or variable according to a 24-hours sine-law; T_{mr} is the ambient mean radiant temperature, assumed equal to T_a under the assumption that the ambient behaves like a black-body; h_c is the coefficient of convection, which, once a wind speed of nearly 2.5m/s is assumed, is taken equal to 15 W/m^{2}K [10]; k is the thermal conductivity; and n denotes the direction normal to the surface element being considered.

As far as the initial condition is concerned, i.e., the thermal field across the integration domain at time τ = 0 when the infrared heater starts scanning the ground surface, an initial uniform temperature $T_0 = T_a$ is assumed in the first-step analysis. On the contrary, the initial condition assumed in the second-step analysis, i.e., when the effects of climate are evaluated, the spatial temperature distribution at time τ = 0 has been determined as follows: (1) a uniform temperature value is assumed across the whole integration domain equal to 15°C, which may be assumed as typical for superficial water tables; (2) both the air temperature and the incoming solar radiation are subjected to the daily cyclic variations reported in Fig. 2 for an overall time-period (of the order of ten days) sufficiently long to eliminate the influence of the original temperature distribution, i.e., up to when the daily percent changes of temperature at any grid-node are smaller than a prescribed value, i.e., 10^{-5}; (3) the spatial thermal field which corresponds to the time of the day at which the heater starts scanning the ground surface is assumed as the temperature field at time τ = 0.

Simulations are performed for the same variety of combinations of the values of A, S, R, P, Q, V, and τ_d, used in part I of the paper, within the same ranges of variability, i.e., 25cm^2 ÷ 350cm^2 for A, 0.5 ÷ 5 for S, 1 ÷ 3 for R, 1cm ÷ 5cm for P, 10W ÷ 10kW for Q, 0.125cm/s ÷ 2.5cm/s for V, and 30s ÷ 2500s for τ_d.

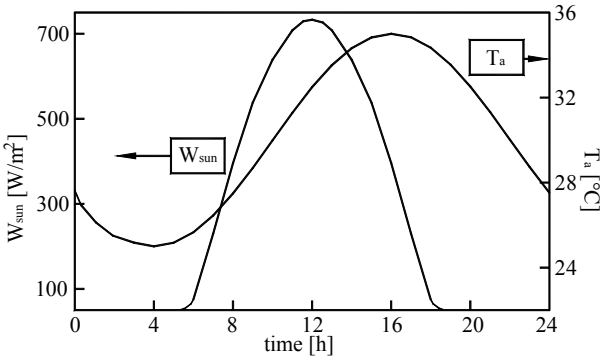

Fig. 2. Time evolution of the air temperature and of the incoming solar radiation on the soil surface per unit area over a diurnal cicle.

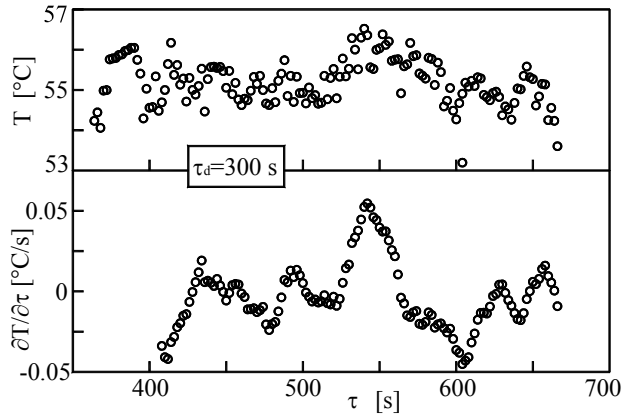

Fig. 3. Thermometer readings and time-derivatives for τ_d=300s.

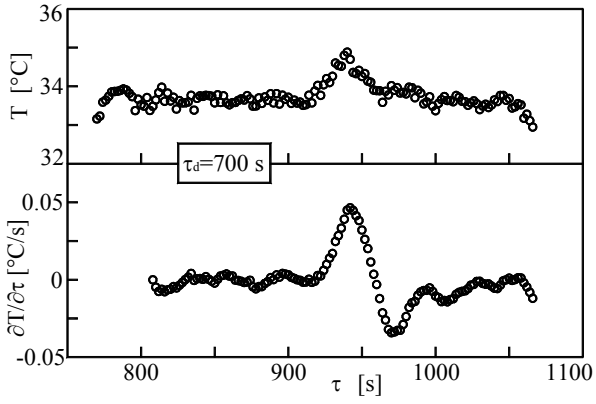

Fig. 4. Thermometer readings and time-derivatives for τ_d=700s.

3 Results and discussion

3.1 Résumé of the main results of part I

The analysis conducted in part I of the paper took into account neither the soil non-uniformity, nor the effects of climate. According to the basic

results obtained, the detection capability of the scanning device proposed increases as: (a) the burial depth P of the landmine decreases; (b) the ratio R = b/a, between the dimension of the irradiated ground surface normal to the scanning direction and the characteristic dimension of the buried landmine, increases; and (c) the energy e absorbed by the unit area of the irradiated ground, given by e = (Q/V)/b where Q = εWA is the IR power absorbed at the irradiated ground surface, increases. In addition, the temperature contrast arising on the soil surface, assumed as indicator of the detection performance of the system, is a non-monotonic function of the delay-time τ_d =d/V, which is the time required to span the distance d between the heated area and the thermometer at the scanning velocity V of the device.

3.2 First-step analysis

Typical time-distributions of the temperature data recorded by the thermometer which follows the heater, and of their time-derivatives, are reported in Figs. 3 and 4, for, e. g., P = 2cm, e= 288J/cm^2, S = 2.5, and R =1, and for delay-times τ_d = 300s and 700s, respectively. Time τ which appears in the abscissa is the time elapsed from the beginning of the ground irradiation. The time-derivatives are obtained by means of the angular coefficient of the line which, instant by instant, interpolates the last twenty temperature readings.

It may be observed that the non-uniformity of the physical properties of the soil generates a scattering of data which may conceal the presence of the buried object, such scattering being more evident for the temperature data than for the time-derivative distributions, which show a well defined peak. However, the degree of concealment of possible temperature anomalies decreases as the delay-time τ_d increases, thus meaning that, in the meanwhile the soil returns to the thermal equilibrium, the temperature gradients which originates from the soil non-homogeneity extinguish more rapidly than those produced by the presence of the buried object.

Owing to the aforementioned scattering of data, the temperature contrast C must necessarily be calculated as the difference between interpolation curves. In particular, C is calculated as the maximum difference between the fourth-degree polynomial which interpolates the temperature data actually recorded by the thermometer, and the linear interpolation of the temperature data recorded far from the perturbed field.

The distributions of C versus the delay-time τ_d, for R =1, and different pairs of values of e and Q, are reported in Fig. 5, for, e.g., P = 4cm.

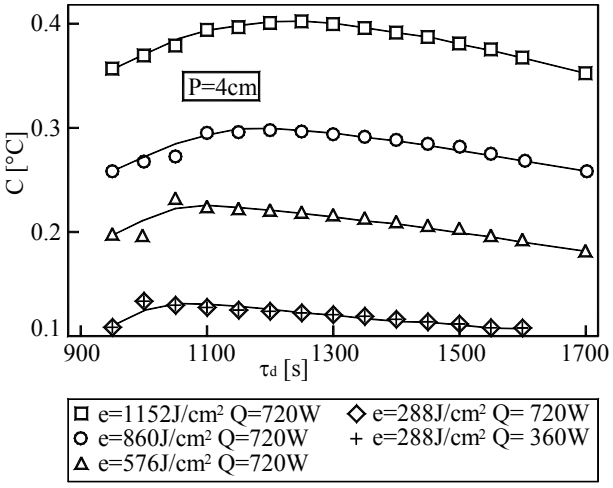

Fig. 5. Distributions of C vs. τ_d for different pairs of values of e and Q, P=4cm, and R=1.

It may be noticed that, as for the case of a homogeneous soil, once P and R are assigned, the temperature contrast is a function of only the energy e absorbed by the unit area of the irradiated ground, and of the delay-time τ_d. Of course, the maximum temperature contrast C_{max} will depend only on e, again according to a substantially linear dependency, as shown in Fig. 6 for, e. g., P = 4 cm, R = 1, and several values of S in the range between 2 and 5. It seems worth noticing that the linear interpolations of the values of C_{max} versus e found at any burial depth investigated, are practically the same as those derived for a uniform soil (by example, the linear distribution of Fig. 6 coincides with the linear distribution for P = 4cm reported in figure n.8 of part I of the paper). However, this occurrence must not lead to the conclusion that the soil non-uniformity has no effect at all.

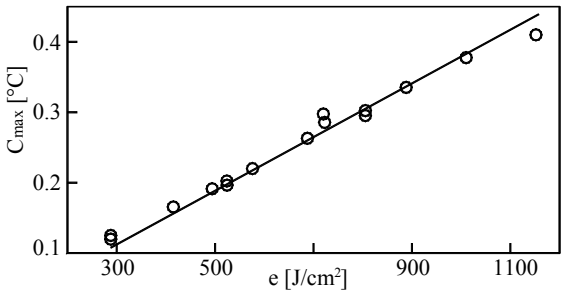

Fig. 6. Distributions of C_{max} vs. e at P=4cm

Actually, owing to the scattering of data discussed above, what matters is not only the strength of the signal picked up, but also its clearness. This means that a signal-to-noise ratio C/δC must be introduced, where δC is the error due to such scattering of data, and that attention must be duly paid to its value. In particular, the value of δC is calculated as the sum of the root-mean square

RMS(1) of the fourth-degree polynomial which interpolates the actual data recording, and of the root-mean square RMS(2) of the linear distribution which corresponds to the unperturbed field. The distributions of C/δC versus the delay-time τ_d for, e. g., the temperature contrast data collected in Fig. 8 are reported in Fig. 7. It may be seen that the values of C/δC at the delay-times corresponding to C_{max} may be very low, even below unity, almost independently of the energy e. As τ_d increases, also C/δC increases, up to reaching a maximum. This would tend to suggest that, for the evaluation of the most suitable delay-time, reference should be made to a sufficiently high value of the signal-to-noise ratio, rather than to the maximum value of the temperature contrast, which was the approach followed for homogeneous soils. On the other hand, even at large values of the delay-time, the signal-to-noise ratio C/δC may be not high enough to be considered as acceptable for a reliable landmine detection, especially at the largest burial depths investigated. In fact, low values of C/δC makes the more deeply buried objects very difficult to be detected, even if considerable temperature contrasts are present. This is, e.g., the case displayed in Fig. 8, where the temperature readings, and their time-derivatives, are reported for P = 4cm, e = 1152J/cm^2, S = 4, and R = 1, and a delay-time τ_d = 1200s. It may be seen that the temperature contrast is strongly concealed by the noisy background, and thus completely useless. On the other hand, the positive peak of the time-derivative of temperature, whose amplitude is denoted as $(\partial T/\partial\tau)_{max}$, can easily be distinguished from the background, proving to be more effective to our purposes. Same type of result has been found for all the situations investigated, thus leading to the conclusion that, for landmine detection in non-uniform soils, the double information brought by both the maximum temperature contrast and the positive peak of the temperature gradient, should be analysed. In this context, also the signal-to-noise ratio $(\partial T/\partial\tau)_{max}/\delta(\partial T/\partial\tau)_{max}$ must be defined, similarly to what has been previously made for C/δC.

The distributions of $(\partial T/\partial\tau)_{max}/\delta(\partial T/\partial\tau)_{max}$ versus the delay-time τ_d for some of the cases discussed in Fig. 8, i. e., for P = 4cm, R = 1, and different pairs of values of e and Q, are reported in Fig. 9. As for the ratio C/δC, also the ratio $(\partial T/\partial\tau)_{max}/\delta(\partial T/\partial\tau)_{max}$ is substantially independent of the energy e, while depending only on the burial depth P. What is really worth noticing is that the values of $(\partial T/\partial\tau)_{max}/\delta(\partial T/\partial\tau)_{max}$ are nearly ten times larger than those of C/δC, which confirms that, whenever in real situations the landmine detection relies also on the value of $(\partial T/\partial\tau)_{max}$, the system is able to ensure same detection capabilities of those found for homogeneous soils. In addition, as for C_{max}, also $(\partial T/\partial\tau)_{max}$ is independent of the value of S. Finally, last but not the least, it must be underlined that, once P and R are assigned, the value of $(\partial T/\partial\tau)_{max}$ does not depend on the scanning velocity V, as shown in Fig. 10, where the distributions of $(\partial T/\partial\tau)_{max}$ versus the delay-time τ_d are reported, for, e. g., P = 1cm, Q = 25W, R =1, and for different values of the scanning velocity V in the range between 0.25cm/s and 2cm/s, and of S in the range between 0.5 and 1. Obviously, the independency of V may represent a true advantage, as possible increases in the scanning velocity may be taken into account for investigation-time reduction, consistently with the resolution of the contactless thermometer adopted.

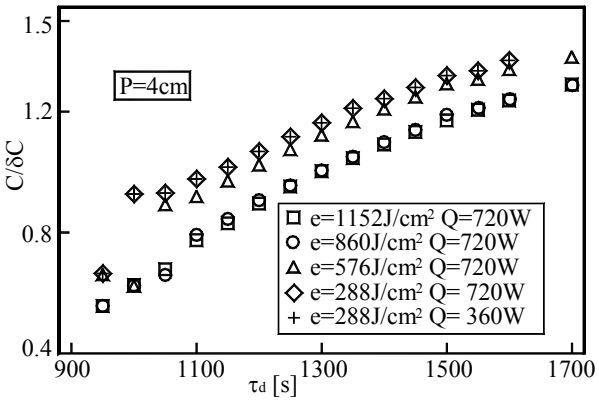

Fig. 7. Distributions of C/δC for different pair of values of e and Q, P=4cm, and R=1.

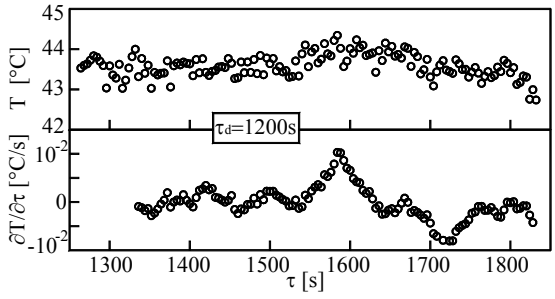

Fig. 8. Thermometer readings and time-derivatives for τ_d=1200s (P=4cm, e=1152J/cm2, S=4, and R=1)

3.3 Second-step analysis

The changes in air temperature and in solar irradiation during the investigation-time give rise to positive temperature contrasts during the day-time, during which the soil surface warms up, and to negative temperature contrasts at night, during which the topsoil cools down.

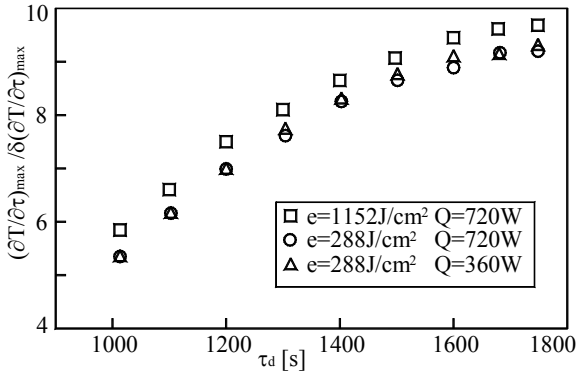

Fig. 9. Distributions of $(\partial T/\partial\tau)_{max}/\delta(\partial T/\partial\tau)_{max}$ vs. τ_d different values of the e-Q, P=4cm, and R=1.

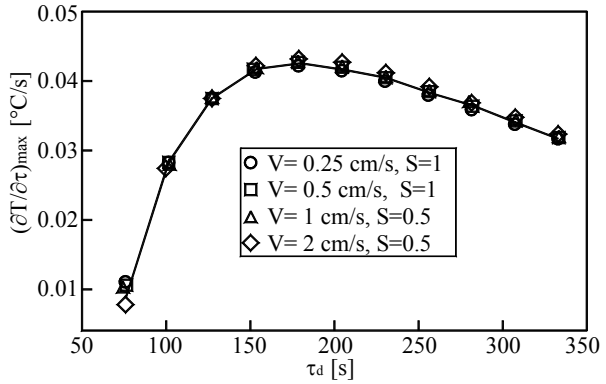

Fig. 10. Distributions of $(\partial T/\partial\tau)_{max}$ vs. τ_d different values V (P=1cm, Q=25W, S=0.5, and R=1).

This is illustrated in Fig. 11, where six snapshots show the temperature evolution of the soil surface below which the landmine is buried at a depth of 1cm. Taking into account that the isotherm spacing is of 0.1°C, the largest temperature contrast detectable above the mine is of 0.3°C, which occurs at 04:00pm. Obviously, such even low contrast is doomed to decrease drastically with increasing the burial depth.

According to this, two different situations arise. In fact, at relatively large burial depths, at any time of the day the contribution of the natural heating is practically negligible with respect to that caused by the IR artificial irradiation. On the other hand, for the smaller burial depths, any time the soil scanning for landmine detection is conducted at night, the negative temperature contrasts induced by the soil cooling are in opposition with the positive temperature contrasts induced by the IR artificial irradiation, which may introduce non-negligible noise in the temperature data. Of course, the temperature data collected during day-time are characterized by a meaningfully smaller amount of noise, as the effects of both the natural and the artificial heating are in agreement. This is shown in Figs. 12 and 13, where the results obtained at 04:00am and at 12:00am, for, e. g., P=3cm, e = 380J/cm^2, S = 3, and R = 1, and a delay-times τ_d = 800s, are reported. However, it may be seen that, even at night, the use of $(\partial T/\partial\tau)_{max}$ allows for good detection performance, as testified by the evident peak of the temperature gradient noticeable in Fig. 12.

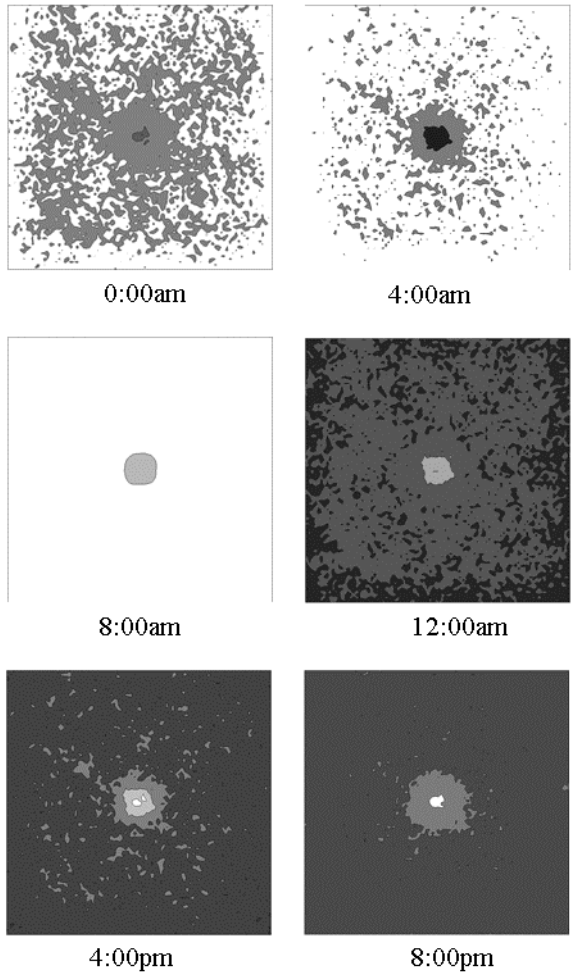

Fig. 11. Thermal field on the ground surface around the mine buried at P=1cm at different hours of the day (the area sketched is 0.45mx0.45m; the temperature difference between two consecutive isotherms is 0.1°C)

The study conducted up until now has assumed that the scanning line of the detection device passed exactly along the symmetry axis of the projection of the buried landmine upon the ground surface. This allowed for the use of just one thermometer, moving along the direction of the symmetry axis of the heater in the scanning direction. Indeed, it may happen that the irradiated ground surface covers only partially the ground surface located right above the buried object. In such case, it seems useful to employ a multi-thermometer device, of the type depicted in Fig.

22, where, e. g., it is assumed that for R = 1 the heater is followed by an array of 5 thermometers, 1cm apart from each other, and that the heated ground surface overlaps only half of the mine projection upon the soil surface.

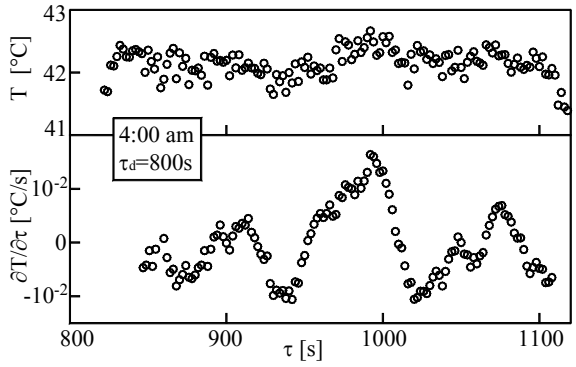

Fig.12. Thermometer readings and time-derivatives at 4.00am for τ_d=800s (P=3cm, e=380J/cm2, S=3, and R=1).

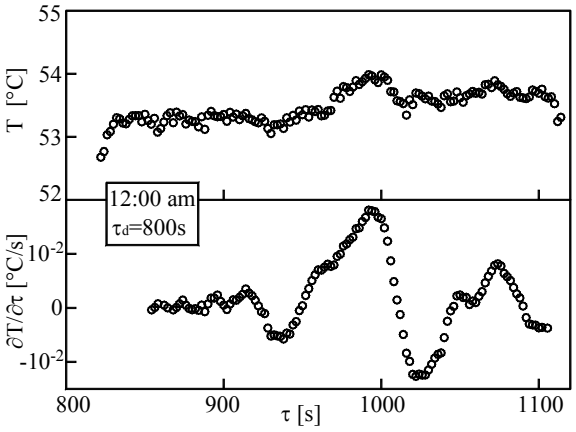

Fig.13. Thermometer readings and time-derivatives at 12.00am for τ_d=800s (P=3cm, e=380J/cm2, S=3, and R=1).

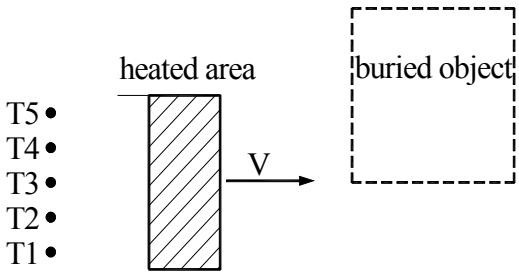

Fig. 14. Sketch of the thermal detector and target geometry for a multi-thermometer configuration.

The results obtained for P = 3cm, e = 480 J/cm^2, S = 4, R = 1, and τ_d = 1000s, are reported in Fig. 15 for thermometers T1, T3 and T5 in terms of time-derivatives of temperature. It may be seen that the signal picked up by thermometer T1 is strongly concealed by the background, but, at the same time, thermometers T3 and T5 are able to spot the mine independently from one another. Same type of result has been obtained for many other situations, thus encouraging about the detection performance of the device proposed.

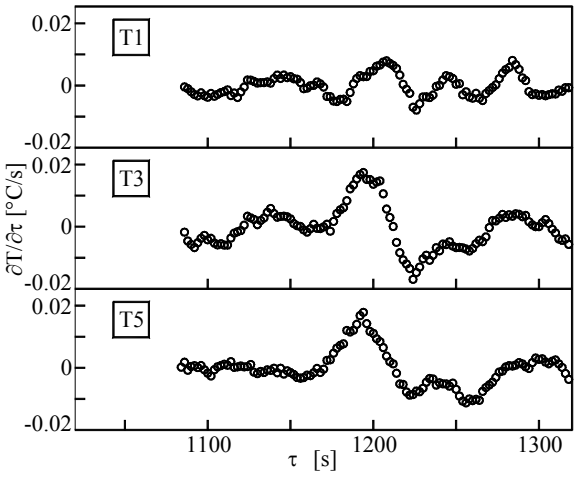

Fig. 15. Data collected by the thermometers T1-T5 and their time-derivatives for partial heating of the ground above the mine (P=3cm, e=480J/cm^2, S=4, R=1, and τ_d=1000s).

4 Constructional aspects

The main components, i.e., the heater and the thermometer, will be discussed first.

As far as the heater is concerned, the infrared source, mounted on the scanning device, must be equipped with a focusing device, as, e.g., a lens, so as to deliver the radiant energy emitted onto a small ground surface. However, since the source is hot, its presence in the proximity of the ground surface could affect the cooling process which follows the heat stimulation. A possible solution to this problem is the adoption of optical fibres to deliver infrared radiation from a distance, which would also avoid the use of the focusing equipment mounted on the scanning device. Optical fibre illuminators, currently used for other purposes, such as microscope lightning, are commercially available.

As concerns the thermometer, industrially available digital infrared pyrometers with miniature sensor head for non-contact temperature measurement without cooling system may be adequate for the task. In fact, they are light, relatively inexpensive, have normally fast response times, and can also reach a resolution of 0.1K. Their accuracy cannot be considered an issue, as the detection method proposed is based on the temperature change rather than on its absolute value. Also stability of measurement need not to be

very tight, since only short-term differences are significant.

The system performance may then be enhanced by a proper post-processing of the signal, such as filtering for noise reduction, application of principal or independent component analysis, or soft computing strategies. In any case a simple reading should be provided to the operator, which might be obtained in the form of an alarm signal triggered by automatic detection of an anomaly in the surface temperature, and/or temperature time-derivative, above pre-assigned threshold values.

Other possible extensions of the basic architecture may include the use of a forward thermometer, and of arrays of heaters.

A thermometer moving before the heater would sense temperature differences of the soil surface along the scanning line, caused by solar irradiation before the artificial IR stimulation is delivered to the ground, which could permit to estimate small space-scale variations, so as to cancel or reduce the noise due to soil variability.

The scanning procedure may then be sped up by using an array of heaters aligned normal to the scanning direction, which would result in a definitely wider heating front-line. Of course, such a set-up would require more power than the basic one discussed above. However, we do not think that a reasonable increase in the power required would drastically limit the portability of the device, which, e.g., could be powered through a cable by a small generator.

Finally, instead of a suspended rail for carrying the heater and/or the thermometers, the use of a lightweight wheeled vehicle travelling on the soil surface may be considered. In fact, such a set-up might permit to follow the ground irregularities much better, although non-negligible efforts are certainly required to force the vehicle to move precisely along a straight path.

5 Conclusions

A performance analysis of the active infrared scanning system for thermal detection of buried landmines introduced in part I of the paper, has been conducted with reference to more realistic situations than those considered before, in order to determine the effects of soil non-uniformities, as well as of solar irradiation and air temperature changes which occur during the investigation-time. Constructional aspects of the device, and possible extensions of the basic architecture, have been proposed and discussed.

The main results obtained may be summarized as follows:

(a) The non-uniformity of the physical properties of the soil generates a scattering of data which may conceal the presence of the buried landmine, such scattering being more pronounced for the temperature data than for those of its time-derivative.

(b) The maximum temperature contrast C_{max} depends linearly on the energy e absorbed by the unit area of the irradiated ground surface, according to the same relation found for a uniform soil. In contrast, the peak of the positive time-derivative of temperature $(\partial T/\partial \tau)_{max}$ depends basically on the power absorbed at the ground surface.

(c) Independently of the delay-time τ_d, the values of the signal-to-noise ratio of the temperature contrast $C/\delta C$ may be not high enough to be considered as acceptable for a reliable landmine detection. In contrast, at any delay-time τ_d, the values of the signal-to-noise ratio for the peak of the positive time-derivative of temperature $(\partial T/\partial \tau)_{max}/\delta(\partial T/\partial \tau)_{max}$ are significantly larger than those of $C/\delta C$, up to nearly ten times. Thus, once the double information brought by both C_{max} and $(\partial T/\partial \tau)_{max}$ is analysed, the system proposed is able to ensure good detection performance also in noisy backgrounds.

(d) Climate effects give rise to positive temperature contrasts during daytime, and to negative temperature contrasts at night, which superimpose to the positive temperature contrast induced by the artificial IR soil heating. However, the noise introduced in the temperature data collected during night-time is never so high to prevent the device proposed to locate AP landmines buried down to a depth of 5cm.

(e) The use of a multi-thermometer device would permit to detect a buried landmine even in case the irradiated ground surface covers only partially the mine projection upon the soil surface.

All things considered, the results of the simulations performed enforce the feasibility of the mine detection device proposed. Of course, both laboratory and field experiments on different types of targets buried in different types of soils, are required, which are the aims of future work.

References

[1] I. K. Sendur, B. A. Baertlein, Numerical simulation of thermal signatures of buried mines over a diurnal cycle, in Detection and Remediation Technologies for Mines and Minelike Targets V, Proceedings of the SPIE, vol. 4038 (2000).

[2] S. Sjokvist, M. Georgson, M. Uppsall, M. Patterson, Temporal IR contrast variation of

buried land mines, in Detection and Remediation Technologies for Mines and Minelike Targets V, Proceedings of the SPIE, vol. 4038 (2000).

[3] P. B. Schewering, A. Kokonozi, J. L. Carter, H. A. Lensen, E. M. Franken, Infrared landmine detection and thermal model analysis, in Detection and Remediation Technologies for Mines and Minelike Targets VI, Proceedings of the SPIE, vol. 4394 (2001).

[4] K. Khanafer, K. Vafai, Thermal analysis of buried land mines over a diurnal cycle, IEEE Transaction on Geosciences and Remote Sensing 40 (2002) 461-473.

[5] P. Soelberg, J. Storm, B. Stage, B. D. Sorensen, Resolution requirements for thermal detection of buried landmines, in Detection and Remediation Technologies for Mines and Minelike Targets V, Proceedings of the SPIE, vol. 4038 (2000).

[6] W. A. Messelink, K. Shutte, F. C. Vossepoel, F. Cremer, J. G. M. Schavamaker, E. den Breejen, Feature-based detection of landmines in infrared images, in Detection and Remediation Technologies for Mines and Minelike Targets VII, Proceedings of the SPIE, vol. 4742 (2002).

[7] J. Stefanic, M. Malinovec, S. Svaic, V. Krstelj, I. Boras, Advanced analysis of thermograms of buried objects in non-homogeneous environment, Proceedings of QIRT2002: Quantitative Infrared Thermography 6 (2002).

[8] J. Stefanic, M. Malinovec, S. Svaic, V. Krstelj, Parametrization of non-homogeneities in buried object detection by means of thermography, Infrared Physics and Technology 45 (2004) 201-208.

[9] P. López, L. van Kempen, H. Sahli, D. C. Ferrer, Improved thermal analysis of buried landmines, IEEE Transactions on Geoscience and Remote Sensing 42 (2004) 1965-1975.

[10] W. C. Mc Adams, Heat transmission, 3rd ed., Mc Graw-Hill, New York, 1954.